ISSN 1070-3632, Russian Journal of General Chemistry, 2015, Vol. 85, No. 5, pp. 1209–1221. © Pleiades Publishing, Ltd., 2015.
Original Russian Text © M.V. Mishin, V.S. Protopopova, S.E. Alexandrov, 2013, published in Rossiiskii Khimicheskii Zhurnal, 2013, Vol. 57, Nos. 3–4, pp. 5–16.

Plasmachemical Synthesis in Low-Temperature Atmospheric Pressure Plasma

M. V. Mishin, V. S. Protopopova, and S. E. Alexandrov

St. Petersburg State Polytechnic University, Politekhnicheskaya ul. 29, St. Petersburg, 195251 Russia
e-mail: mmishin@spbstu.ru; vera_protopopova@mail.ru; salexandrov@spbstu.ru

Received January 1, 2013

Abstract—Pesicular features of various types of electrical gaseous discharges used to generate and sustain low-temperature plasma at atmospheric pressure have been considered. Applications of dielectric barrier discharges (DBD), corona, radiofrequency (RF), and microwave (MW) discharges for the synthesis of different materials have been discussed.

DOI: 10.1134/S1070363215050394

INTRODUCTION

Nonequilibrium low-temperature plasma is characterized by significantly higher electron energies compared to the energies heavy plasma components: ions, neutral atoms, and molecules. Collisions of high-energy electrons with atoms and molecules result in their dissociation, excitation, and ionization. It is worth to mention that these processes are not accompanied by a considerable increase of the temperature of heavy plasma component. Due to the fact that ionized and neutral plasma components remain to be relatively low energetic plasma does not cause the thermal effect on the substrate surfaces.

Nonequilibrium low-temperature plasma is easily generated in electrical discharge at low pressure. However, this technology has a serious disadvantage, namely, the need in a costly vacuum equipment.

In this connection, beginning in mid-1990s, much effort has been made all over the world on the development of low-temperature plasma sources stably working at atmospheric pressure. Since this time the number of publications on low-temperature atmospheric pressure plasma (LTAPP) sources has become to grow exponentially. Most LTAPP sources are relatively simple and have fairly low operating costs. The use of sources operated at high partial pressures of precursors (about three orders of magnitude higher compared to low-pressure plasma), brings great advantages to plasmachemical processes involving homogeneous chemical reactions, for example, plasma enhanced chemical vapor deposition (PECVD) of nanopowders or cleaning from toxic organic compounds. However, certain problems with LTAPP sources arise in plasma assisted processes based on heterogeneous chemical reactions (PECVD of thin films or etching of materials) due to the necessity to prevent homogeneous reactions leading to vapor phase depletion or by-product formation. At the same time, recent research has shown that LTAPP holds promise for practical applications: film deposition, synthesis of new compounds, surface modification, removal of highly toxic organic pollutants from air, surface etching, synthesis of nanopowders, etc.

Most LTAPP sources are based on arc discharges characterized by high heat release. Arc discharge plasma is widely used in technology (welding, sawing, sputtering, and high-temperature chemical synthesis). However, such thermal strains might be reasonable high for many applications, because the temperature of the treated surface can reach 2000°C. In this connection, over the past twenty years active R&D work has been done on plasma sources with different types of electrical gaseous charges (corona, barrier, radiofrequency, and microwave), with lower temperatures of heavy plasma components (600–800°C).

In present review work we will demonstrate the great horizons of using low-temperature atmospheric pressure plasma processes for plasma stimulated synthesis of different materials.

Specific Features of Electrical Gaseous Discharges at Atmospheric Pressure

The gaseous discharges at low pressures (0.5–200 Pa) are widely used for generation of low-temperature plasma and can sustain over a long time. It happens due to the fact that the characteristic time of the discharge instability development which induces to transition of the glow discharge to arcing is indefinitely long. The usage of atmospheric pressure leads to shortening the time of discharge instability development up to nanoseconds [1].

Abundant evidence is available [2–26] to show that any processes that tilt balance between generation and lack of charge carriers can cause instability and the transition from volume discharge to channeling. This transition results in a change of the temperature regime and in spatial inhomogeneity of plasma, which is critical and highly undesirable for many technological applications. Furthermore, another reason for the instability of the atmospheric pressure plasma during the nanomaterial synthesis is the accumulation of plasmachemical reaction products having lower ionization potentials and, consequently, higher ionization rates [27].

Discharge instability is the main limiting factor to the design of sources of low-temperature nonequilibrium volume discharges at atmospheric pressure, and this prompts research into the reasons for their generation and mechanisms of development [4, 5, 7].

The main problem that must be solved when developing LTAPP sources is to stabilize and sustain discharge in the reaction gas mixture. A general approach is either the usage of an inverse feedback for the discharge current–voltage or restriction of the discharge sustainability time.

Most modern plasma sources use self-sustained atmospheric pressure gaseous discharge. As the largest amplitude of electric field in self-sustained plasma is in the cathode region, the instabilities are associated with field fluctuations initiated in this region. Several methods to suppress electric field fluctuations have been reported [28–35]. The simplest one [28] is the use of a segmented cathode with each segment connected to power supply source via a ballast resistor. The fluctuations of the discharge current (for example, increase), induced by developing discharge instabilities, lead to fluctuations (increase) of the voltage, which drops on the ballast resistor, and, consequently, changes (decrease) the discharge voltage. Another approach to avoid instabilities in the cathode region is establishing such discharge sustainability conditions that prevent plasma formation in this plasma region. For this purpose, another discharge region, which plays the role of the cathode region for the main volume plasma zone, were added [29–35]. Plasma cathodes are efficient in terms of suppression of cathode potential drop and are capable of ensuring reliable contact with plasma, because they are not damaged by secondary processes on their surface. However, the processes that occur in the double layer at the plasma boundary, can induce instabilities as well [28].

A fairly simple approach to preventing the transition of the volume discharge to channeling can be realized in the case of corona discharge [36]. Corona discharge takes place when a high electric field with a potential gradient (strength) is created near at least one of the electrodes. This condition is fulfilled when an electrode contains prickly parts with a small curvature radius (tip or needle). The corona discharge current is confined by the space charge of carriers in the strength region. The charge carriers drift to the second electrode (ideally, at infinity) in the gas under the action of the electric field. The corona discharge can be generated and sustained both at a dc and ac over a wide range of frequencies. Pulsed corona discharges, where non-equilibrium plasma is formed due to streamers propagating from a needle electrode, are also used [37, 38].

The use of such gas discharges in the plasma-chemical technology is limited by a strong spatial inhomogeneity of plasma. The region, where the most intense gas ionization and excitation processes take place, is localized in the vicinity of the tip electrode. In the case when a substrate to be treated is placed close to a high-voltage corona-producing electrode, special measures should be taken to prevent short-circuiting the discharge current to the substrate and discharge sparking or arching (depending on the power supply source).

An alternative approach to prevention of discharge instabilities consists in limiting the time of discharge current flowing less than the transition time from the volume discharge to channeling [7, 28, 39–65].

The discharge time can be limited by using a dielectric barrier on the electrode surface. The dielectric

Process parameters of electric discharges for generation of low-temperature plasma and its characteristics [67, 87, 88]

Type of discharge	Process parameters				Characteristics of plasma		
	frequency, MHz	input power, W	power density, W/cm^3	gas flow rate, L/min	electron temperature, eV	electron density, cm^{-3}	gas temperature, K
RF low-temperature	1–40	20–500	3–30	0.5–50	1–4	10^{11}–7×10^{12}	300–700
DBD diffusion mode	5×10^5–5×10^2	10–2000	0.5–1	1–10	3–5	10^{11}–5×10^{11}	300–500
Streamer mode	5×10^5–5×10^2	20–1000	1–50	0.2–5	1–10	10^{14}–10^{15}	300–400
Corona	0.001–1		1–50	0.5–4	3–7	10^9–10^{13}	300–400
MW	2.45×10^6	10^2–10^3		1–20			300–400

barrier discharge (DBD) [63] is generated if there is at least one insulating dielectric barrier in the discharge gap between plane or cylindrical ac electrodes. The discharge gap thickness can vary from 0.1 to 10 mm, and the applied frequency, from hundreds of Hz to GHz. The materials of insulating layers (dielectric barriers) are most commonly glass, quartz, ceramics, as well as thin enamel and polymeric coatings on metal electrodes. Such dielectric barrier discharges are defined as sustained in microdischarge (or streamer mode) [64, 65]. In this case, the discharge occurs in a large number of streamers formed due to the electric field caused by local charge accumulation on the dielectric barrier surface [64]. The propagation of streamers from one electrode to the other results in recharging of the dielectric surface, which reverses the applied field polarity and leads to streamer streamer current drop.

There is another discharge mode in barrier discharge plasma sources, specifically the diffuse mode [54–59]. In contrast to the streamer mode, it is uniformly distributed over the entire discharge gap. It was shown that discharge is sustained by a series of current pulses a few microseconds in length. The reasons why the volume discharge does not shift to channeling mode in this case (discharge pinching) and the mechanisms responsible for high spatial uniformity of discharge are still to be established conclusively. The stability of the diffuse DBD plasma is independent on the gas flow rate and depends on the applied frequency (in the kHz range), nature and composition of the gas mixture, and supplied power. The most sustainable DBD discharge was obtained in helium and other gases (argon, nitrogen, air) [29–33, 65].

The the electrode gaps in DBD plasma sources are about a few mm. The ion concentration in the volume plasma is usually 10^{10} cm^{-3} but sometimes reaches 10^{12} cm^{-3} [34, 35].

It is worth noting that the discharge time can be limited by controlling the gas flow rate through the discharge region [58–60]. For discharge stabilization the plasma-forming gas was supplied at a linear rate of ~10^2 m/s. In this case, the residence time of gas molecules in the plasma is equally important as the pulse time. If there are critical zones in the discharge gap, the high-rate gas flow can favorably affect the perturbation sources in these zones and thus stabilize the discharge [40–50].

One the past years considerable progress has been achieved in the development of sources of non-equilibrium low-temperature plasma by using high-frequency discharge [66–79]. A stable volume atmospheric pressure glow discharge between two metal electrodes can be generated in pure helium or chemically active gases strongly diluted with helium, by applying voltage with a frequency of 13.56 MHz on the electrodes. If there is a dielectric barrier on one of the electrodes, discharge can be sustained in argon or its dilute mixtures with other gases (nitrogen, oxygen, etc.).

Gas discharges at atmospheric pressure can also be sustained using higher frequency (up to microwave) power supply sources. Such plasma sources are most frequently used in analytical spectroscopy, because the discharge gap in them is no larger than 1 cm [80–86].

The table lists the process parameters and characteristics of electrical gaseous discharges at atmospheric

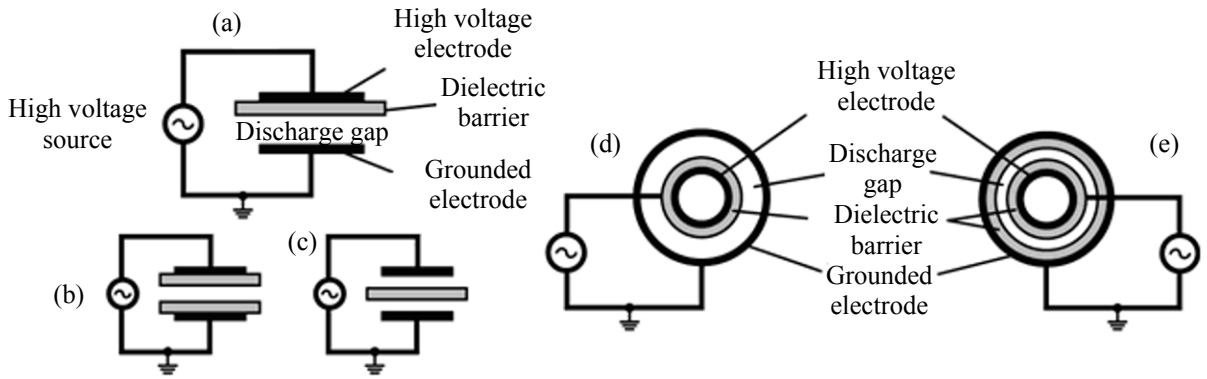

Fig. 1. Schematics of DBD chambers. Electrode arrangement: (a, b, c) plane parallel and (d, e) coaxial.

pressure, that are the most widely used in plasma-chemical technologies.

Application of the Dielectric Barrier Discharge in the Plasmachemical Synthesis of Nanomaterials

Dielectric barrier discharge (is one of the most common methods of generation of nonequilibrium AP plasma. Reactors for DBD can have a plane parallel (Figs. 1a–1c) or a coaxial (Figs. 1d, 1e) electrode configuration, but the most characteristic feature of such reactors in both cases is the presence of an insulating dielectric barrier layer on one or both electrodes and a short distance between the electrodes (≤5 mm). The frequencies used for DBD generation and sustainability typically are in the range 50 Hz to 300 kHz. The amplitude of the ac voltage applied to electrodes is 5–15 kV.

Owing to their hardware simplicity and reliability, DBD plasma sources have found wide application in the synthesis of materials. The variety of the designs of DBD reactors is explained by the diversity of tasks to be solved and materials to be synthesized, including not only thin films but also nanostructured materials [65, 89, 90].

Nozaki et al. [91, 92] reported attempted synthesis of carbon nanotubes (a promising material for field-emission cathode applications) in the reaction chamber with a plane parallel electrode system (Fig. 1a). In this case, the dielectric barrier for a hot (maximum temperature 700°C), lower electrode was an alumina ceramic plate 1 mm in thickness. The upper electrode worked as a gas distributor (helium, hydrogen, and methane) fed at the rates 0.9 L/min, 100 mL/min, and 10 mL/min, respectively. The width of the discharge gap was 4 mm, and the applied frequency was 10–100 kHz. However, the authors of the cited work failed to synthesize vertically aligned carbon nanotubes at such an electrode configuration. With both positive and negative voltages, the synthesis led to a carbon material containing a small amount of nanotubes and a soot-like carbon.

Kyung and co-workers [93, 94] achieved deposition of carbon nanotube arrays, employing the upper electrode with a more complicated design (Fig. 1b). A characteristic feature of this design was that the dielectric barrier at the upper electrode (a ceramic plate 10 mm in thickness) were perforated (hole diameter 1 mm). Such design allows high-density plasma channels to form in the holes through which the gases mixture are fed in. The dielectric barrier at the lower electrode was a quartz plate 3 mm in thickness. Carbon nanotubes were synthesized at deposition temperatures of 400°C. The discharge gap was 5 mm. The applied voltage had a frequency of 20–100 kHz and an amplitude of 3 kV. The gas mixture consisted of acetylene (90 mL/min) and ammonia (60 mL/min), and the plasma-forming gas was helium (6 L/min). Under optimal synthesis conditions, arrays of vertically aligned but bended carbon nanotubes up to 2 μm in length and 20–50 nm in average diameter formed. However, during the synthesis a thick carbon layer was formed on top of array led to termination of CNT growth, the reasons for which have not been explored, unfortunately.

Another original task solved using DBD plasma, is depositing coatings on nanoparticles. Lei et al. [95] described successful deposition of a protective film of hydrogenated carbon on 10–100-nm copper nanoparticles by using the DBD plasma technology. The nanoparticle synthesis and their coating were performed in a two-zone reactor. Copper nanoparticles

were synthesized by sputtering a copper wire in an inductively coupled plasma (ICP) at atmospheric pressure. The synthesized particles were transported with an argon carrier gas flow to the other reactor zone, where the gas mixture of methane and hydrogen (working gases to form the carbon coating) was supplied. The DBD plasma was generated in a reactor with a coaxial electrode configuration (Fig. 1d). The width of the discharge gap was 8 mm at the channel length of 30 cm. Alternating voltage (amplitude 15 kV, frequency 20 kHz) was applied to the high-frequency electrode. The gas flow rates were as follows: argon 5 L/min, hydrogen 2 L/min, and 1 L/min. The thickness of the deposited hydrogenated carbon film was 10–20 nm. Fourier transform IR spectroscopy gave evidence showing that the resulting fims are polymers and contain CH, CH_2, and CH_3 functional groups. Such coating prevents oxidation of the nanoparticles on their contact with air (metal nanoparticles are highly sensitive to oxidation, which creates problems with their synthesis).

One more nontrivial task which can be solved with the use of DBD reactors with a coaxial electrode configuration is depositing coatings on cylindrical objects. Prat et al. [96] reported the deposition of fluorocarbon polymers on glass tubes. The electrodes were two isolated copper strips wound on the external side of the tube reactor. High voltage (5 kV, 20 kHz) was applied on one of the electrodes, and the other electrode was grounded. The reagents were tetrafluoroethylene and hexafluoropropylene. According to IR and X-ray fluorescence spectral data, the chemical composition of the synthesized polymer was close to that of poly(tetrafluoroethylene). Under optimal conditions (tetrafluoroethylene and helium flow rates 2.5 mL/min, helium flow rate 0.6 L/min), the deposition rate was 50 nm/min.

Along the specific tasks of nano-object coating and deposition of uniform layer into trenches or pores as objects with a complicated shape, there is a need to deposit thin films with a uniform composition and thickness onto planar objects with a large surface area. Such tasks can be solved to success by means of the DBD plasma exited in reactors with a plane parallel electrode configuration. Goossens et al. [97] obtained polymeric coatings from the gas mixture with ethylene with the discharge initiated between two disk aluminum electrodes (Fig. 1b) coated with an alumina film (alternating voltage amplitude 20 kV, frequencies 1 and 4 kHz). Films were deposited onto different substrates mounted on the grounded electrode. The plasma-forming gas was helium or argon with a total flow rate of 1–20 L/min. Ethylene (the reagent gas) was supplied with a 20-fold dilution. As shown, the polymers synthesized in a helium plasma form low-density colored viscous coatings, whereas those synthesized in an argon plasma form transparent, hard, and well adhesive coatings. The deposition rates were 100 nm/min with helium and 20 nm/min with argon. The composition of the resulting polymer depends on the type of the substrate, but the product was always structurally similar to polyethylene. Other applications of the barrier discharge for polymer coating deposition are given in [98–101].

Along with polymer deposition, atmospheric pressure DBD can be used for activation of chemical vapor deposition of various inorganic materials.

Davis et al. [102] studied titanium dioxide film deposition in a horizontal tube reactor with two plane parallel electrodes isolated with quartz plates. The discharge was sustained by applying alternating voltage (frequency 33 kHz, amplitude 10 kV) to the high-voltage electrode. The plasma-forming gas was helium (3 L/min). The reagents were oxygen (5 mL/min) and titanium tetrachloride carried by helium (0.5 L/min). Titanium dioxide films were deposited on cold substrates at a rate of 70 nm/min. The films had a a granular structure (grain size 50–300 nm).

Rymuza et al. [103] synthesized silicon nitride films in a deposition setup with plane parallel electrodes. High voltage (12.5–15 kV, 5 kHz) was applied to the external electrode. The electrode gap width was 1–2 mm. The lower, grounded electrode was heated. The deposition temperature was 300–400°C. The total gas flow was 150 mL/min. The reagent was hexamethyldisilazane whose vapor was carried (0.0045%) from the external chamber by nitrogen. The deposition rate was 5–10 nm/min. The IR and X-ray fluorescence spectral data showed that the resulting film consists of hydrogenated silicon nitride, sometimes with an oxygen contamination. Atomic force microscopy revealed a smooth film with the maximum roughness height ~11 nm.

In view of the high deposition rates, DBD plasma can be used for continuous film deposition, for instance, onto a moving tape [100, 104]. O'Neill et al. [100] obtained silicon diioxide films in a reactor with plane parallel electrode configuration (50 × 10 cm). A voltage of 8 kV (frequency 30 kHz) was applied to the

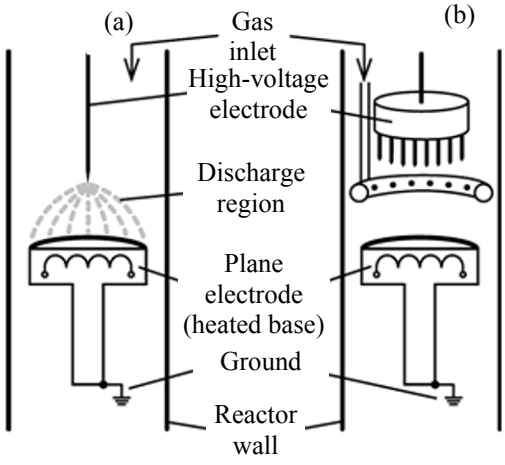

Fig. 2. Schematics of corona discharge chambers with (a) one needle electrode and (b) several electrodes.

high-voltage electrode. The plasma-forming helium gas flow rate was 15 L/min, the oxygen flow rate was 100 mL/min, and the flow rate of the organosilicon reagent was 10–12.5 mL/min. Films were deposited onto substrates moving at a rate of 4 m/min. It was shown that continuous films formed from poly(dimethylsiloxane, the use of tetraethoxysilane and octamethylcyclotetrasiloxane as precursors gave films and a small amount of powder, whereas with the usage of tetramethylcyclotetrasiloxane and tetramethyldisiloxane, much nanopowder resulted. According to X-ray fluorescence spectral data, the film composition was close to $SiO_{1.9}$.

Review of the synthesis possibility of various materials in atmospheric pressure DBD showed that this type of discharge allows decreasing the deposition temperature. Thus, for example, carbon nanotubes were synthesized at 400–700°C, whereas in the case of heat-enhanced chemical vapor deposition, heating wafers to 650–1050°C is required. Oxide and nitride film deposition occurs at much lower temperatures (300–400°C) and sometimes at room temperatures. This method of the synthesis of polymer coatings at room temperature holds promise for large-scale commercialization. The high film growth rates reached in certain processes (up to 200 nm/min) provide evidence for the practical perspective of such technologies.

However, this method is not free of certain disadvantages. A uniform atmospheric pressure DBD is not always possible to initiate and sustain, and this may result in a nonuniform film thickness across the substrate surface. Furthermore, the fact that substrates are located directly in the discharge region may, in view of the small electrode gap, leads to defect formation in the growing film due to bombardment by high-energy plasma speciees.

Application of the Corona Discharge in the Plasmachemical Synthesis of Nanomaterials

Atmospheric pressure plasma-enhanced chemical vapor deposition (AP-PECVD) of various materials with the use of corona discharge has found fairly wide application [18, 27, 104–108].

Reactors designed for this technology contain at least one needle electrode (Fig. 2a) or a comb with several needle electrodes (Fig. 2b) [108].

The authors of [18, 27, 104] described a simply designed electrode system comprising a needle electrode located axially to a vertical reactor and a plane, grounded electrode located perpendicularly to the reactor axis; high voltage (2.8–8 kV, 25-50 kHz) was applied to the upper electrode. This reactor was used to synthesize carbon nanotubes at room temperature (reagent gases hydrogen and methane, total flow rate 22 mL/min) [104].

To improve the uniformity and homogeneity of deposited films, Thyen et al. [107] proposed a modernized upper electrode constructed of four needle electrodes each embedded in an alumina tube which plays the role of a dielectric barrier. The lower electrode is made from aluminum coated with polytetrafluoroethylene. High voltage is applied to the needle electrodes (10–20 kV, frequency 20–50 kHz), and the lower electrode is grounded. The process gases are supplied through gas showers, each placed between two needle electrodes.

The described reactor was used to deposit nonstoichiometric silicon dioxide films from tetramethylsilane or tetraethoxysilane and oxygen. The plasma-forming gases were argon and nitrogen. The highest apparent deposition rate was 500 nm/min. However, at such high rates homogeneous powder formation took place, and, the resulting films were loose and had poor mechanical characteristics. Smooth and hard films were obtained at deposition rates not higher than 100 nm/min. The O/Si ratios in the films varied from 2.2 to 2.5, and their hydrogen contents ranged from 20 to 29 at %. The same reactor was also used to synthesize hydrogenated carbon films from hydrocarbons (CH_4, C_2H_2, etc.).

A principal possibility to synthesize nanocarbon films using dc corona discharge, even though such

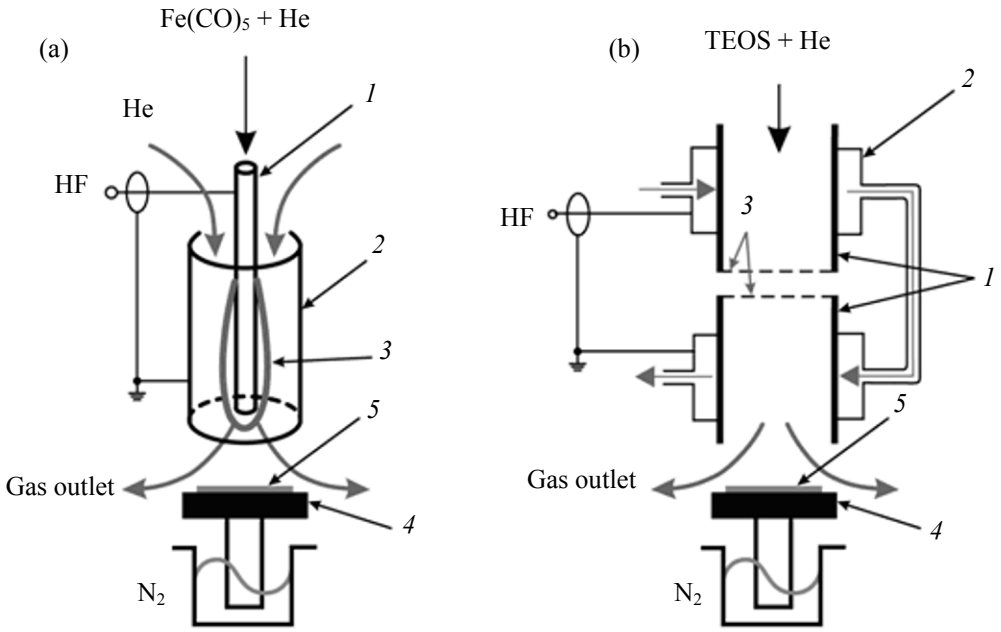

Fig. 3. Schematics of reactors with (a) coaxial electrodes: (*1*) internal hollow electrode; (*2*) external electrode; (*3*) discharge region; (*4*) cold base plate; and (*5*) wafer [118] and (b) plane parallel electrodes: (*1*) electrodes; (*2*) electrode water cooling; (*3*) gauzes; (*4*) cold base plate; and (*5*) wafer [119].

discharges are fairly seldom used for activation of chemical processes, was demonstrated in [109] and [110]. The design of the reactor used in these works is similar to that in Fig. 1a. High voltage (up to 10 kV) is applied to a needle electrode, the second, plane electrode is grounded, and the electrode gap is 10 mm. Discharge initiated at voltages not lower than 3.3 kV. The reactor is heated with a resistance oven, the maximum temperature is 700°C. The reagents are ethanol or hexane and hydrogen. The resulting layers were structures comprising a flaky carbon. The Raman spectra showed that they might contained nanotubes and graphene layers.

Corona discharge can be successfully used for the synthesis of nano-objects (carbon nanotubes, flaky carbon, silicon dioxide layers, etc.) at room temperatures. The disadvantage of this technique consists in spatial nonuniformity of the discharge, which leads to nonuniformity of the resulting coatings, as well as their nonstoichometric composition. The reproducibility of the composition and properties of the deposited films is unsatisfactory, because corona discharge is difficult to control.

Application of Radiofrequency Discharges in the Plasmachemical Synthesis of Nanomaterials

Over the past decade radiofrequency (RF) discharges have received wide recognition in plasma-enhanced deposition technologies. Syntheses can be performed in reactors with a plane parallel electrode configuration. Substrates may be placed both directly in the plasma region [93, 111] and beyond this region (so-called remote plasma processes) [112–118]. Certain tasks seem to be better solved in reactors with coaxial electrodes [119].

In [119] we used a reactor with remote low-temperature plasma generated with a system of coaxial electrodes (Fig. 3) to synthesize iron-containing nanoparticles [119]. The applied power was varied in the range 0–100 W, voltage frequency 13.56 MHz, plasma-forming gas (helium), flow rate 2–2.4 L/min. The reagent iron pentacarbonyl, its vapor was transferred to the reactor by a carrier gas (helium) fed with the flow rate 0–30 mL/min.

Dependences of certain RF discharge characteristics on process parameters (in particular, discharge

(a) (b)

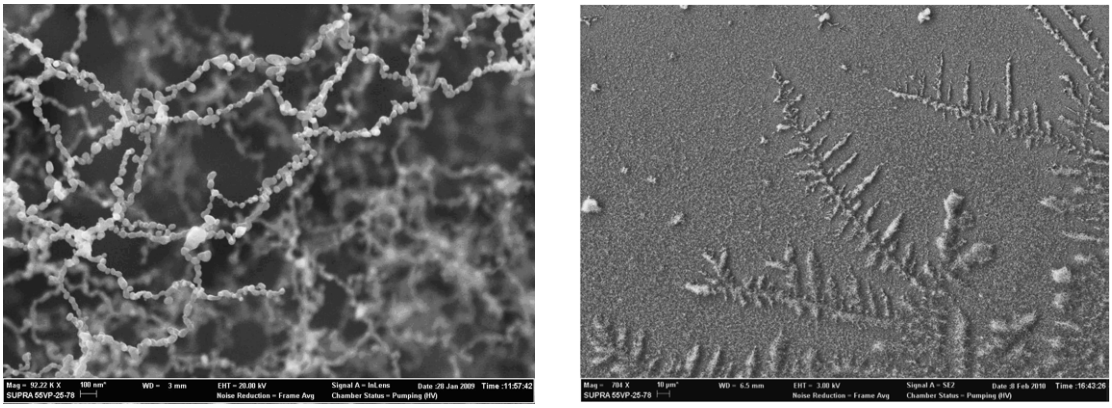

Fig. 4. Microscopic images of nanoparticles synthesized in reactors with (a) coaxial (power 65 W) [118, 120] and (b) plane parallel electrodes [119, 120]. The fractal dimentions of the structures in the images are close to 1.7.

power supply) were studied. Its voltage–current characteristic was obtained and conditions of its existence in the α- and γ-modes were determined. It was shown that at low applied voltages the α-mode is realized, at which the current is formed by avalanche multiplication of carriers. Once the voltage (i.e. absorbed power in the discharge) has increased above a certain threshold value, the discharge current jumps upwards abruptly and transition to a γ-mode discharge is observed. This transition is accompanied by sheath breakdown and initiation of a more efficient mechanism of carrier multiplication, specifically, secondary ion–electron emission, as evidenced by the dependences of internal electrode temperature and integral plasma radiation intensity power absorbed in the discharge. Thus, beginning with the absorbed power of about 30 W, a sharp rise of the central electrode temperature took place, whereas the visible and UV radiation intensity rose only slightly.

The described technique was used to synthesize iron-containing nanoparticles with the characteristic sizes ranging from 5 to 80 nm (irrespective of the discharge mode), which formed complex agglomerates (Fig. 4a). The average size of the nanoparticles decreased with increasing partial pressure of the reagent (in the α-mode). The rate of nanoparticle formation in the γ-mode was 1.3×10^{-2} mg h^{-1} cm^{-2} and was about double that observed in the α-mode (1.2×10^{-3} mg h^{-1} cm^{-2}). The experiments in [119] gave evidence to a non-unifom distribution of electric field between coaxial electrodes and the resulting fast development of discharge instability.

A more stable RF discharge (13.56 MHz) could be obtained in a system with plane parallel electrodes (Fig. 3b) [117] made from metal meshes or perforated and then anodized aluminum disks. The absorbed power was varied from 1–40 W. This system was tested for the synthesis of silicon dioxide nanoparticles from tetraethoxysilane (TEOS). The gas mixture was supplied from the top to a quartz reactor (diameter 20 mm) directly to the discharge zone. The plasma-forming gas (helium) flow rate was varied in the range 100–450 mL/min, and the flow rate of the carrier gas supplied through the evaporator was varied from 50 to 200 mL/min. The synthesized particles were deposited onto different substrates at room or liquid nitrogen temperature. Scanning electron microscopy showed that the product consisted of 8–16-nm particles. These particles formed fractal structures on the surface (Fig. 4b). Analysis of the correlation between the morphology of the coating with the deposition process parameters and plasma characteristics showed that surface diffusion processes are much affected by the charge of the synthesized nanoparticles [118].

Low-temperature atmospheric pressure RF plasma was used to success in the synthesis of dense films of various materials.

The authors of [112–116] used a deposition set-up in which remote RF plasma was generated between perforated plane parallel electrodes. The characteristic feature of the set-up was that the gas mixture could be introduced both directly to the discharge and to the afterglow zone. This set-up was used to synthesize diamond-like films, silicon oxides and nitrides, zinc oxide, and amorphous silicon.

Diamond-like films were synthesized by directly delivering the reaction gas mixture to the RF plasma

zone (27.12 MHz, 160 W) [112]. The plasma-forming gas was helium (30 L/min), and the reagent gases were hydrogen (0.5 L/min) and acetylene (50–100 mL/min). The substrate temperature was varied from 100 to 400°C. The deposition rate decreased from 0.3 to 0.7 μm/min as the substrate temperature increased from 100 to 400°C. The deposited films comprised sp^2 and sp^3 carbons.

Films of other materials were conveniently synthesized when the plasma-forming gas and reagents were supplied separately. Thus, in the synthesis of zinc oxide [113] helium (plasma-forming gas) was fed (30 L/min) to the discharge zone, while carbon monoxide or oxygen (44 mL/min) and diethylzinc (20–70 mTorr), to the afterglow zone. At the maximum partial pressure of the reagent (70 mTorr), the growth rate of zinc oxide particles was 120 nm/min at the substrate temperature 100°C. It was shown that in the absence of plasma activation the particle growth rate in the same conditions was about half as low.

The same deposition setup was used to synthesize silicon nitride films [114]. Helium and nitrogen were fed to the discharge zone (13.56 MHz, 50–62 W) and silane, to the afterglow zone. The deposition rate increased from 9 to 130 nm/min as the substrate temperature was increased from 100 to 500°C. Changing the N_2/SiH_4 ratio from 55 to 5.5 resulted in that the compositions of the resulting films were different from stoichiometric (from $SiN_{1.45}$ to $SiN_{1.2}$). The lowest contents of the carbon (0.04%), oxygen (3.6%), and hydrogen (13.6%) impurities were obtained at the deposition temperature 500°C and the N_2/SiH_4 ratio 22.

Hydrogenated silicon films were synthesized under the same conditions but with a mixture of silane and hydrogen [116]. The helium and hydrogen flow rates were 40 L/min and 0–920 mL/min, respectively. The highest film growth rate of 12 nm/min was reached at the deposition rate of 450°C and the hydrogen, silane, and helium partial pressures of 6.3, 0.3, and 778 Torr, respectively. The deposition rate increased with increasing reagent partial pressures and exponentially decreased with increasing electrode–substrate holder distance. The hydrogen content of the resulting films was 2.5– 8 at %.

Nowling et al. [115] demonstrated the possibility of depositing glassy silicon dioxide films from organosilicon reagents and oxygen. Helium (30.6 L/min) and oxygen (2%) were fed directly to the RF plasma zone (27.12 MHz, 100 W) and the reagent (partial pressure 1–1000 mTorr), to the afterglow zone. Hexamethyldisilazane, hexamethyldisiloxane, tetramethyldisiloxane, tetramethylcyclotetrasiloxane, and tetraethoxysilane were tested as reagents. The highest deposition rate of 910 nm/min was observed with tetramethyldisioxane (100 mTorr), but such films had the highest contents of hydroxy groups (by IR spectroscopy). With the other reagents, the growth rates were 15–250 nm/min and increased as their partial pressures increased. The lowest contents of impurities (OH and CH_x) were observed with hexamethyldisilazane.

Comparison of the results obtained in the two last-mentioned groups of works on the atmospheric pressure RF plasma enhanced synthesis of nanoparticles and solid films shows that nanoparticles are formed at relatively low flow rates of working gases and dense solid films are formed at orders-of-magnitude higher gas flow rates.

A more stable discharge and denser plasma can be obtained using higher voltages with higher frequencies. Such highly stabilized discharges have made possible epitaxial growth of semiconductor films. Kirihata et al. [120] synthesized silicon and boron-doped silicon epitaxial films in a system constructed of plane parallel electrode with a porous carbon upper electrode. The gas mixture comprising helium (50 L/min), hydrogen (35 mL/min), silane (35 mL/min), and diborane (0.01–20 mL/min) was fed from the porous carbon. Plasma was initiated and sustained in the discharge gap of 0.8 mm, high voltage (1.2 kV, frequency 150 MHz) was applied to the upper electrode.

A system with a high-speed rotating upper electrode was tested [121]. The substrate temperature in all experiments was 470–700°C, which is much lower compared to the temperatures characteristic of thermally activated chemical vapor deposition (CVD) of silicon particles (950–1250°C). The highest particle growth rates reached with this technique were 6.6 μm/min at 690°C and 1.2 μm/min at 610°C, which is several times faster than in the CVD process (0.2–0.3 μm/min).

The resulting data allow us to conclude that the high-frequency RF discharge technology holds much promise for high-speed deposition of various coatings, including epitaxial films, onto moving substrates.

Atmospheric pressure RF discharges can be used to prepare carbon nanotube arrays. Comparison of the results of synthesis of carbon nanotubes in atmospheric pressure DBD and RF (13.56 MHz) plasmas [91, 111]

showed that in the first case no carbon nanotube arrays formed, while in the second case at the same temperature (700°C) quality arrays of vertically aligned carbon nanotubes could be obtained. Moreover, according to [111], atmospheric pressure RF plasma has symmetric regions of a cathodic ion sheath and a dark space.

Other examples of application of RF discharges in the synthesis of various materials can be found in [122–126].

Thus, the use of RF plasma allows much lower deposition temperatures and high-speed deposition. Moreover, RF discharge makes it possible to generate plasma at a distance from the substrate and to perform selective reagent activation. The latter seems especially important because to generate plasma in the immediate vicinity of the substrate is undesirable in most processes because ions bombard the surface of the substrate and the growing film, thus producing defects in the resulting material.

Application of Microwave Discharges in Plasmachemical Synthesis

Microwave (MW) discharges were used to success in plasma-assisted deposition of various materials at atmospheric pressure.

Brown et al. [127] described a system for continuous deposition of silicon films (50–400 nm) on carbon fibers. A quartz T-shaped reactor with a top sleeve for continuously feeding carbon fiber and a perpedicular sleeve for connecting a waveguid for MW power (power 2 kW, frequency 2.45 GHz). Nitrogen was supplied to the plasma region, and the reagent was fed to a region remote from the plasma region.

Cardoso et al. [128] reported silica film deposition using remote MW plasma. Discharge was generated in a quartz tube (diameter 27 mm) embedded into a waveguide. The absorbed power (frequency 2.45 GHz) was 435 W. Discharge was initiated in an Ar/O_2 mixture. The reagent (hexamethyldisiloxane) was fed directly to the substrate surface through an alumina needle. The substrate (diameter 30 mm) was placed 7.6 cm apart from the resonator and perpendicularly to the gas flow.

Research on the effect of the substrate temperature on the film thickness uniformity showed that increasing temperature decreases the characteristic reaction time between the reagent and active plasma species. As a result, the maximum film thickness shifts toward the needle, i.e. to the region corresponding to shorter times of contact between hexamethyldisiloxane and active plasma components.

Other applications of MW plasma in the synthesis of films of various materials are described in [129, 130].

CONCLUSIONS

The present review on the use of low-temperature plasma initiated by electric discharges in gases at atmospheric pressure for activation of various syntheses provides evidence showing that plasma-chemical technologies hold much promise and are attractive for commercialization on an industrial scale. Such processes offer the advantages of a fairly low cost of equipment and a high efficiency of technologies due to, among other things, higher partial pressures of reagents compared to those applied in plasmachemical processes at low pressures.

The considered types of discharges can be used to success in the plasmachemical synthesis of powders, films, and coatings. Of undeniable interest is the application of low-temperature plasma for plasmachemical etching, synthesis of nanomaterials (nanoparticles, carbon nanostructures, etc.) and polymers, epitaxial film growing, waste treatment, etc.

REFERENCES

1. Kunhardt, E.E. and Luessen, L., *Electrical Breakdown and Discharges in Gases. Part A: Fundamental Processes and Breakdown*, New York: Plenum, 1981.
2. Nigham, W.L. and Wiegand, W.J., *Phys. Rev*., 1974, vol. A10, pp. 922–945.
3. Velikhov, E.P., Pis'mennyi, V.D., and Rakhimov, A.T., *Sov. Phys. Usp*., 1977, vol. 20, pp. 586–602.
4. Cernak, M., Hosokawa, T., and Inoshima, M., *Appl. Phys. Lett*., 1990, vol. 57, pp. 339–340.
5. Kushner, M.J., *IEEE Trans. Plasma Sci*., 1991, vol. 19, no. 2, pp. 387–399.
6. Botticher, W., Luck, H., Niesner, St., and Schwabedissen, A., *Appl. Phys*., 1994, vol. 76, no. 9, pp. 5036–5047.
7. Kulikovsky, A.A., *J. Phys. D: Appl. Phys*., 1993, vol. 26, pp. 431–435.
8. Ul'yanov, K.N., *Zh. Tekh. Fiz*., 1973, vol. 43, no. 3, pp. 570–577.
9. Baranov, V.Yu. and Ul'yanov, K.N., *Zh. Tekh. Fiz*., 1969, vol. 39, no. 2, pp. 249–258.
10. Eletskii, A.V., *Khim. Plazmy*, 1982, no. 9, p. 151.
11. Eletskii, A.V. and Starostin, A.N., *Fiz. Plazmy*, 1976, vol. 2, pp. 838–842.

12. Bychkov, V.L. and Eletskii, A.V., *Fiz. Plazmy*., 1988, vol. 14, p. 1497.
13. Kovalev, A.S. and Persiantsev, I.G., *Pis'ma Zh. Tekh. Fiz*., 1980, no. 12, pp. 743–747.
14. Kanatenko, M.L., *Pis'ma Zh. Tekh*., 1983, vol. 9, no. 4, pp. 214–218.
15. Genkin, S.A., Korolev, Yu.D., Mesyats, G.A., Rabotkin, B.G., and Khuzeev, A.P., *Teplofiz. Vys. Temp*., 1982, vol. 20, pp. 1–5.
16. Genkii, S.A, Kozyrev, A.V, Korolev, Yu.D., et al., *Zh. Tekh. Fiz*., 1985, vol. 55, no. 6, pp. 1216–1218.
17. Bychkov, Yu.I., Genkin, S.A., Korolev, Yu.D., et al., *Vestn. Vyssh. Uchebn. Zaved., Fizika*, 1978, vol. 10, pp. 146–149.
18. Douglas-Hamilton, D.H. and Mani, S.A., *J. Appl. Phys*., 1974, vol. 45, pp. 4406–4416.
19. Kostylev, A.A., Londer, Y.I., Terent'ev, A.P., and Ul'yanov, K.N., *Sov. Phys. Tech. Phys*., 1977, vol. 17, no. 2, pp. 193–200.
20. Hill, R.D., *J. Appl. Phys*., 1975, vol. 46, pp. 2910–2915.
21. Eletskiy, A.V., Starostin, A.N., et al., Fiz. Plazmy, 1975, vol. 1, no. 4, pp. 684–690.
22. Golubovskii, Y.B. and Zonnenburg, R., *Sov. Phys. Tech. Phys*., 1980, vol. 25, pp. 1220–1222.
23. Akishev, Yu.S., Zakharchenko, A.I., Gorodnicheva, I.I., et al., *Prikl. Mekh. Tekh. Fiz*., 1981, no. 3, pp. 10–13.
24. Karlau, H.E. and Muller, K.G., *IEEE Trans. Plasma Sci*., 1986, vol. PS-14, pp. 603–608.
25. Novak, J.P. and Bartnikas, R., *J. Appl. Phys*., 1988, vol. 64, pp. 1767–1775.
26. Osipov, A.I., Uvarov, A.B., Vinnichenko, H.A., and Roshchina (Sakharova), N.A., *Nelin. Mir*., 2005, nos. 1–2, pp. 40–47.
27. Napartovich, A.P., *Plasmas Polym*., 2001, vol. 6, pp. 1–14.
28. Beaulieu, A.J., *Appl. Phys. Lett*., 1970, vol. 16, pp. 504–506.
29. Roth, J.R., *Industrial Plasma Engineering: Volume 1: Principles*, Bristol: IOP, 1995.
30. Decomps, Ph., Massines, F., and Mayoux, C., *Acta Phys. Univ. Comen*., 1994, p. 47.
31. Massines, F., Gadri, R.B., Descomps, Ph., Rabehi, A., Segur, P., and Mayoux, C., *Proc. XXII Int. Conf. on Phenomena in Ionized Gases*, Hoboken, USA, 1995, vol. 363, pp. 306–315.
32. Trunec, D, Brablec, A., and Stastny, F., *Contrib. Plasma Phys*., 1998, vol. 38, pp. 435–445.
33. Massines, F., Rabehi, A., Descomps, P., Gadri R.B., Segur, P., and Mayoux, C., *J. Appl. Phys*., 1998, vol. 83, pp. 2950–2957.
34. Kunhardt, E.E., Becker, K., and Amorer, L., *Proc. XII Int. Conf. on Gas Discharges and Their Applications*, Greifswald, Germany, 1997, p. 87.
35. US Patent 2000/002225, publ. 13.01.2000.
36. Ming-wei, L., Zheng, H., Xi-zhang, W., Qiang, W., and Yi, C., *Thin Solid Films*, 2003, vol. 435, pp. 116–119.
37. Ming-wei, L., Zheng, H., Xi-zhang, W., Qiang, W., Yi, C., and Yi-Ling, T., *Diamond Relat. Mater*., 2004, vol. 13, pp. 111–115.
38. Endo, M., Takeuchi, K., Iagrashi, S., Kobori, K., Shiraishi, M., and Kroto, H.W., *J. Phys. Chem. Solids*, 1993, vol. 22, no. 17, pp. 1213–1224.
39. Morrison, R.W. and Swail, C., *Phys. Lett*., 1972, vol. 40A, pp. 375–377.
40. Hidson, D.J., Makios ,V., and Morrison, R.W., *Phys. Lett*., 1972, vol. 40A, pp. 413–414.
41. Tan, K.O., Makios, V., Morrison, R., and Tea, W.A., *Phys. Lett*., 1972, vol. 38A, pp. 225–226.
42. Eckbreth, A.C. and Davis, J.W., *IEEE J. Quant. Electron*., 1972, vol. 8, issue 2, pp. 139–144.
43. Fenstermacher, C.A., Nutter, M.J., Leland, W.T., and Boyer, K., *Appl. Phys. Lett*., 1972, vol. 20, pp. 56–60.
44. Nakamura, K., Yukawa, N., and Mochizuki, T., *Appl. Phys. Lett*., 1986, vol. 49, pp. 1493–1495.
45. Alexandrov, V.Y., Gurevich, D.B., Kulagina, L.V., Lebedev, M.S. and Podmoshenskii, I.V., *Sov. Phys. Tech. Phys*., 1975, vol. 20, pp. 62–67.
46. Apollonov, V.V., Mininkov, V.R., and Prokhorov, A.M., *Sov. J. Quant. Electron*., 1984, vol. 14, pp. 898–901.
47. Slade, P.D. and Serafetinides, A., *IEEE J. Quant. Electron*., 1978, vol. QE-14, pp. 321–322.
48. Gibson, A.F., Hall, T.A., and Hatch, C.B., *J. Quant. Electron*., 1977, vol. QE-13, pp. 801–803.
49. Hill, A., *Appl. Phys. Lett*., 1971, vol. 18, pp. 194–197.
50. Eckbreth, A.C. and Davis, J.W., *Appl. Phys. Lett*., 1972, vol. 21, pp. 25–27.
51. Palmer, A.J., *Appl. Phys. Lett*., 1974, vol. 25, pp. 138–140.
52. Levatter, J.I. and Lin, S.C., *Appl. Phys. Lett*., 1980, vol. 51, pp. 210–223.
53. Bondarenko, A.V., Lebedev, F.V., and Smakotin, M.M., *Pis'ma Zh. Exp. Teor, Fiz*., 1982, vol. 8, no. 11, pp. 648–653.
54. Gadri, R.B., *IEEE Trans. Plasma Sci*., 1999, vol. 27, no. 1, pp. 36–37.
55. Kanzawa, S., Kogoma, M., Okazaki, S., and Moriwaki, T., *Nuclear Inst. Methods Phys. Res*., 1989, vol. B37, pp. 842–845.
56. Yokoyama, T., Kogoma, M., Kanzawa S., Moriwaki, T., and Okazaki, S.J., *J. Phys. D: Appl. Phys*., 1990, vol. 23, pp. 374–377.
57. Yokoyama, T., Kogoma, M., Moriwaki, T., and Okazaki, S.J., *J. Phys. D: Appl. Phys*., 1990, vol. 23, pp. 1125–1128.
58. Okazaki, S. J., Kogoma, M., Uehara, M., and Kimura, Y., *J. Phys. D: Appl. Phys*., 1993, vol. 26, pp. 899–892.

59. Kogoma, M. and Okazaki, S.J., *J. Phys. D: Appl. Phys*., 1994, vol. 27, pp. 1985–1987.
60. Akishev, Yu.S., Deryugin, A.A., Kochetov, I.V., Napartovich, A.P., and Trushkin, N.L., *J. Phys. D: Appl. Phys*., 1993, vol. 26, pp. 1630–1637.
61. Akishev, Yu.S., Deryugin, A.A., Karal'nik, V.B., and Kochetov, I.V., et al., *Plasma Phys. Rep*., 1994, vol. 20, pp. 511–524.
62. Akishev, Yu.S., Deryugin, A.A., Elfin, N.N., Kochetov, I.V., et al., *Plasma Phys. Rep*., 1994, vol. 20, pp. 437–441.
63. Kogelschatz, U., *IEEE Trans. Plasma Sci*., 2002, vol. 30, no. 4, pp. 1400–1408.
64. Eliasson, B. and Kogelschatz, U., *IEEE Trans. Plasma Sci*., 1991, vol. 19, pp. 309–322.
65. Kogelschatz, U., Eliasson, B., and Egli, W., *J. Phys. IV France*, 1997, vol. 7, pp. C4-47–C4-66.
66. Selwyn, G.S., *Plasma Proc. Polym*., 2007, vol. 4, pp. S487–S492.
67. Schütze, A., Jeong, J.Y., Babayan, S.E., Park, J., et al., *IEEE Trans. Plasma Sci*., 1998, vol. 26, pp. 1685–1694.
68. Jeong, J.Y., Babayan, S.E., Tu, V.J., Park, J., et al., *Plasma Sources Sci. Technol*., 1998, vol. 7, pp. 282–285.
69. Babayan, S.E., Jeong, J.Y., Tu, V.J., and Park, J., *Plasma Sources Sci. Technol*., 1998, vol. 7, no. 3, pp. 286–288.
70. Selwyn, G.S., Herrmann, H.W., Park, J., and Henins, I., *Contrib. Plasma Phys*., 2001, vol. 41, pp. 610–619.
71. Park, J., Henins, I., Herrmann, H.W., Selwyn, G.S., et al., *Appl. Phys. Lett*., 2000, vol. 76, p. 228.
72. Park, J., Henins, I., Herrmann, H.W., and Selwyn, G.S., *J. Appl. Phys*., 2000, vol. 89, pp. 15–20.
73. Park, J., Henins, I., Herrmann, H.W., and Selwyn, G.S., *J. Appl. Phys*., 2000, vol. 89, pp. 20–28.
74. Laimer, J., Haslinger, S., Meissl, W., Hell, J., and Störi, H., *Vacuum,* 2005, vol. 79, pp. 209–214.
75. Laimer, J. and Störi, H., *Plasma Proc. Polym*., 2006, vol. 3, pp. 573–586.
76. Li, H-P., Sun, W-T.,Wang, H-B.. Li, G., and Bao, C-Y., *Plasma Chem. Plasma Proc*., 2007, vol. 27, pp. 529–545.
77. Moravej, M., Yang, X., Nowling, G.R., Chang, J.P., and Hicks, R.F., *J. Appl. Phys*., 2004, vol. 96, pp. 7011–7018.
78. Yang, X., Moravej, M., Nowling, G.R., Chang, J.P., and Hicks, R.F., *IEEE Trans. Plasma Sci*., 2005, vol. 33, pp. 314–320.
79. *http://www.surfxtechnologies.com* (June 1, 2012).
80. Beenakker, C.I.M., *Spectrochim. Acta*, 1976, vol. 31B, pp. 483–486.
81. Michlewicz, K.G., Urh, J.J., and Carnahan, J.W., *Spectrochim. Acta*., 1985, vol. 40B, pp. 493–499.
82. Deutsch, R.D. and Hieftje, G.M., *Appl. Spectrosc*., 1985, vol. 39, pp. 214–222.
83. Faires, L.M., Bieniewski, T.M., Apel, Ch.T., and Niemchzk, T.M., *Appl. Spectrosc*., 1985, vol. 39, pp. 5–9.
84. Haas, D.L. and Jamerson, J.D., *Spectrochim. Acta*, 1987, vol. 42B, pp. 299–307.
85. Sofer, I., Zhu, J., Lee, H., Antos, W., and Lubman, D.M., *Appl. Spectrosc*., 1990, vol. 44, pp. 1391–1398.
86. Arkhipenko, V.I., Zgirovskii, S.M., Simonchik, L.V., Smetanin, E.A., and Solov'yanchik, D.A., *Appl. Spectrosc*., 1994, vol. 61, pp. 680–683.
87. Alexandrov, S.E. and Hitchman, M.L., *Chem. Vap. Dep*., 2005, vol. 11, pp. 457–468.
88. Roth, J.R., *Industrial Plasma Engineering: Applications to Nonthermal Plasma Processing*, Institute of Physics Publishing, 2001, vol. 2.
89. Kogelschatz, U., *Pure Appl. Chem*., 1990, vol. 62, pp. 1667–1674.
90. Kogelschatz, U., *Plasma Phys. Control. Fusion*, 2004, vol. 46, pp. B63–B75.
91. Nozaki, T. and Okazaki, K., *Plasma Proc. Polym*., 2008, vol. 5, pp. 300–321.
92. Nozaki, T., Ohnishi, K., Okazaki, K., and Kortshagen, U., *Carbon,* 2007, vol. 45, pp. 364–374.
93. Kyung, S., Lee, Yo., Kim, Ch., Lee, J., and Yeom, G., *Thin Solid Films*, 2006, vols. 506–507, pp. 268–273.
94. Kim, Ch., Lee, Yo., Kyung, S., and Yeom, G., *J. Korean Phys. Soc*., 2005, vol. 46, no. 4, pp. 918–921.
95. Lei, H., Tang, Y., Li, J., Luo, J., and Zhang, J., *Appl. Phys. Lett*., 2009, vol. 91, pp. 113119-1-3.
96. Prat, R., Koh, Y.J., Babukutty, Y., Kogoma, M., et al., *Polymer*, 2000, vol. 41, pp. 7355–7360.
97. Goossens, O., Dekempeneer, E., Vangeneugden, D., Van de Leest, R., and Leys, C., *Surf. Coat. Tech.,* 2001, vols. 142–144, pp. 474–481.
98. Donohoe, K.G. and Wydenven, T., Abstracts of Papers, *4th Int. Symp. on Plasma Chemistry (ISPC-4),* Zurich, Switzerland, 1979, p. 765.
http://134.147.160.41/ ispcdocs/ispc4/DB2.html
99. Reitz, U., Salge, J.G.H., and Schwarz, R., *Surf. Coat. Technol*., 1993, vol. 59, pp. 144–147.
100. O'Neill, L., O'Hare, L.A., Leadley, S.R., and Goodwin, A.J., *Chem. Vap. Dep*., 2005, vol. 11, pp. 477–479.
101. Paulussen, S., Rego, R., Goossens, O., Vangeneugden, D., and Rose, K., *Phys. D: Appl. Phys*., 2005, vol. 38, p. 568.
102. Davis, M.J., Tsanos, M., Lewis, J., Sheel, D.W., and Pemble, M.E., *Electrochemistry,* vol. 203, p. 2173.
103. Rymuza, Z., Misiak, M., Rzanek-Boroch, Z., et al.,

Thin Solid Films, 2004, vol. 466, pp. 158–166.

104. Li, M.W., Hu, Z., Wang, X., Wu, Q., and Chen, Y., *J. Mater. Sci. Lett*., 2003, vol. 22, pp. 1223–1224.
105. Marafee, A., Liu, Ch., Xu, G., Mallinson, R., and Lobban, L., *Ind. Eng. Chem. Res*., 1997, vol. 36, pp. 632–637.
106. Li, M., Hu, Z., Wang, X., Wu, Q., Lu, Y., and Chen, Y., *Chinese Sci. Bull*., 2003, vol. 48, no. 6, pp. 534–537.
107. Thyen, R., Weber, A., and Klages, C.-P., *Surf. Coat. Tech*., 1997, vol. 97, pp. 426–434.
108. Kanazawa, S., Kogoma, M., Moriwaki, T., and Okazaki, S., *J. Phys. D*, 1988, vol. 21, pp. 838–843.
109. Mesko, M., Vretena, V., Kotrusz, P., Hulman, M., et al., *Phys. Status Solidi*., 2012, vol. B249, no. 12, pp. 2625–2628.
110. Yu, K., Bo, Z., Mao, S., Lu, G., et al., *Nanoscale Res. Lett*., 2011, vol. 6, pp. 202–211.
111. Nozaki, T., Goto, T., Okazaki, K., and Ohnishi, K., *J. Appl. Phys*., 2006, vol. 99, p. 024310.
112. Ladwig, A.M., Koch, R.D., Wenski, E.G., and Hicks, R.F., *Diamond Relat. Mater*., 2009, vol. 18, no. 9, pp. 1129–1133.
113. Barankin, M.D., Gonzalez, E., Ladwig, A.M., and Hicks, R.F., *Sol. Energy Mater. Sol. Cells*, 2007, vol. 91, pp. 924–930.
114. Nowling, G.R., Babayan, S.E., Jankovic, V., and Hick, R.F., *Plasma Sources Sci. Technol*., 2002, vol. 11, pp. 97–103.
115. Nowling, G.R., Babayan, S.E., Yajima, M., Moravej, M., et al., *Plasma Sources Sci. Technol*., 2005, vol. 14, pp. 477–484.
116. Moravej, M., Babayan, S.E., Nowling, G.R., Yang, X., and Hick, R., *Plasma Sources Sci. Technol*., 2004, vol. 13, pp. 8–14.
117. Alexandrov, S.E., Kretusheva, I.V., Mishin, M.V., and Yasenovets, G.M., *J. Nanosci. Nanotechnol*., 2011, vol. 11, pp. 7969–7973.
118. Mishin, M.V., Alexandrov, S.E., Kretusheva, I.V., and Boricheva, I.K., *Nauch. Tekh. Vedom. Sankt-Peterb. Gos. Pedagog. Univ., Nauka Obraz*., 2012, no. 4, issue 159, pp. 105–110.
119. Alexandrov, S.E., Kretusheva, I.V., and Mishin, M.V., *ECS Trans*., 2009, vol. 25, no. 8, pp. 943–951.
120. Kirihata, Y., Nomura, T., Ohmi, H., Kakiuchi, H., and Yasutake, K., *Surf. Interface Anal*., 2008, vol. 40, pp. 984–987.
121. Mori, Y., Yoshii, K., Yasutake, K., Kakiuchi, H., et al., *Thin Solid Films*, 2003, vol. 444, pp. 138–145.
122. Barankin, M.D., Creyghton, Y., and Schmidt-Ott, A., *J. Nanoparticle Res*., 2006, vol. 8, pp. 511–517.
123. Inomata, K., Ha, H., Chaudhary, K.A., and Koinuma, H., *Appl. Phys. Lett*., 1994, vol. 64, pp. 46–49.
124. Mori, T., Tanaka, K., Inomata, T., Takeda, A., and Kogoma, M., *Thin Solid Films*, 1998, vol. 316, pp. 89–92.
125. Ogawa, S., Takeda, A., Oguchi, M., Tanaka, K., et at., *Thin Solid Films*., 2001, vol. 386, pp. 213–216.
126. Mori, Y., Yoshii, K., Yasutake K., Kakiuchi, H., et al., *Thin Solid Films*., 2003, vol. 444, pp. 138–145.
127. Brown, M., Hayes, P., and Prangnell, Ph., *Composites*, 2002, vol. A33, pp. 1403–1408.
128. Cardoso, R.P., Belmonte, T., Henrion, G., Gries, T., and Tixhon, E., *J. Appl. Phys*., 2010, vol. 107, p. 024909-1-7.
129. Sugiyama, K., Kiyokawa, K., Matsuoka, H., Itou, A., et al., *Thin Solid Films*, 1998, vol. 316, pp. 117–122.
130. Kiyokawa, K. , Itou, A., Matsuoka, H., Tomimatsu, M., and Sugiyama, K., *Thin Solid Films*., 1999, vol. 345, pp. 119–123.